to have perfect images in each patient. There are several physical obstacles that are difficult to overcome, such as the very poor transmission of sound through air that intervenes between the sound transducer on the body surface and areas of interest within the body. However, other problems appear to be more tractable. These include the appearance of "speckle," problems with inhomogeneous media, and problems with multiple reverberations. Speckle is a grainy pattern, most visible in uniform interior regions of organs such as the liver. Because of the coherent nature of ultrasound, reflections from adjacent scatterers within a small region can interfere constructively or destructively to produce the resulting pattern. This random addition and subtraction of scattered wave fronts creates a mottled appearance that is often interpreted as a property of the tissue involved. Unfortunately, this pattern may obscure a true lesion that is immersed within this noisy environment. There are relatively few studies of this phenomenon although it is now attracting interest. Since the speckle patterns are random, one approach to reducing this effect is to sum a number of images taken from different positions or to use different frequencies to image the same tissue. The resultant speckle will be reduced by the square root of the number of independent images in such a system.

For echo imaging systems, the propagation velocity and attenuation of sound are assumed to be constant. However, variations in velocity and attenuation can seriously distort the sound beam and degrade the image. One possible approach to this problem is the use of variable time-delay devices within phased array systems; the delays could be manipulated to partially compensate for velocity variation and hence to minimize the resultant distortion. Also, images taken from different angles could be combined to minimize distortion.

Echo imaging systems are based on the assumption that the first echo originating from an organ or scatterer is the only echo received with significant intensity. It is assumed that other echoes in this area result from multiple reverberations or reflections of the wave front bouncing back and forth between nearby interfaces. Because the primary reflection is a very small percentage of the transmitted energy, multiple reflections become vanishingly small. However, in a few select cases involving bone or regions containing gas, the reflections are high enough to become visible and must be considered. Clinical operators have learned to recognize and deal with such reverberations by creating images from different transducer positions. Nevertheless, these considerably distort the primary image and may obscure an area of interest.

References and Notes

1. P. N. T. Wells, *Biomedical Ultrasonics* (Academic Press, London, 1977), pp. 110-137.
2. R. L. Popp, *Circulation* **54**, 538 (1976).
3. J. M. Griffin and W. L. Henry, *ibid.* **49**, 1147 (1974).
4. R. C. Eggleton, H. Feigenbaum, K. W. Johnston, A. E. Weyman, J. C. Dillon, S. Chang, in *Ultrasound in Medicine*, D. White, Ed. (Plenum, New York, 1975), vol. 1, p. 385.
5. N. Bom, C. Lancee, G. vanZweiten, F. E. Kloster, J. Roelandt, *Circulation* **48**, 1066 (1973).
6. C. M. Ligtvoet, J. Ridder, C. Lancee, F. Hagemeijer, W. B. Vletter, in *Echocardiography*, N. Bom, Ed. (Nijhoff, The Hague, 1977), pp. 313-323.
7. O. T. von Ramm and F. L. Thurstone, *Circulation* **53**, 258 (1976).
8. W. A. Anderson, J. T. Arnold, L. D. Clark, W. T. Davids, W. J. Hillard, W. J. Lehr, L. T. Zitelli, in *Ultrasound in Medicine*, D. White and R. Brown, Eds. (Plenum, New York, 1977), vol. 3B.
9. A. Macovski and S. J. Norton, in *Acoustical Holography*, N. Booth, Ed. (Plenum, New York, 1975), vol. 6, pp. 121-143.
10. R. P. Martin, H. Rakowski, J. H. Kleiman, W. Beaver, E. London, R. L. Popp, *Am. J. Cardiol.* **43**, 560 (1979).
11. P. M. Nichol, B. W. Gilbert, J. A. Kisslo, *Circulation* **55**, 120 (1977).
12. G. Wade, R. K. Mueller, M. Kaveh, in *Computer Aided Tomography and Ultrasonics in Medicine* (North-Holland, New York, 1979), pp. 165-215.
13. J. F. Greenleaf, S. A. Johnson, S. L. Lee, G. T. Herman, E. H. Wood, in *Acoustical Holography*, P. S. Green, Ed. (Plenum, New York, 1974), vol. 5, pp. 591-603.
14. J. F. Greenleaf, S. A. Johnson, W. F. Samayoa, F. A. Duck, in *ibid.*, vol. 6, pp. 71-90.
15. R. K. Mueller, M. Kaveh, R. D. Iverson, in *Acoustical Imaging* (Plenum, New York, 1980), vol. 8, pp. 615-628.
16. D. Baker, G. Lorch, S. Rubenstein, in *Echocardiology*, N. Bom, Ed. (Nijhoff, The Hague, 1977), pp. 207-221.
17. M. Brandestini, in *ibid.*, pp. 257-265.

18. We thank Barbara Carroll, Linda Joynt, and F. Graham Sommer for contribution of data used in this manuscript. This work was supported in part by grant HL-21278 of the National Heart, Lung, and Blood Institute and grant GM-17940 of the National Institute of General Medical Sciences.

Three-Dimensional Imaging of Heart, Lungs, and Circulation

E. L. Ritman, J. H. Kinsey, R. A. Robb, B. K. Gilbert, L. D. Harris, E. H. Wood

The viability of humans and animals is critically dependent on virtually continuous motions of blood and gases. These motions are generated by movements of all the individual structural components of the circulatory and respiratory systems. Accurate understanding of the interrelationships of these coordinated movements requires synchronous measurements of the changes in shape, dimensions, and position of an entire anatomic structural system simultaneously with its physiologic functions. An example of such an interrelationship is the change in shape and dimensions of the thorax and lungs and the simultaneous spatial distribution of pulmonary ventilation.

Inability to simultaneously measure these parameters and their interrelationships has limited the insights that can be obtained regarding their integrated physiologic functions in the intact organism. This inability has also limited understanding of the multifaceted mechanisms by which various abnormalities, such as coronary artery disease, affect these functions.

The dynamic spatial reconstructor (DSR) was designed to increase insights into physiologic and pathophysiologic interrelationships between anatomic structural dynamics and the corresponding physiologic functions. It is an x-ray imaging device that operates on the principle of computed tomography (CT) and

The authors are all members of the Biodynamics Research Unit of the Department of Physiology and Biophysics at Mayo Medical School, Rochester, Minnesota 55901. E. L. Ritman is associate professor of physiology and internal medicine, J. H. Kinsey is assistant professor in biophysics, R. A. Robb is associate professor in biophysics, B. K. Gilbert is assistant professor in physiology and biophysics, L. D. Harris is assistant professor in biophysics, and E.H. Wood is professor in physiology and internal medicine.

0036-8075/80/1010-0273$01.50/0

Summary. A new imaging device, the dynamic spatial reconstructor (DSR), is described. It differs from commercially available computed tomography scanners in several ways. It images a volume rather than a slice; it images the volume in stop-action to minimize blurring due to motion; and it repeats the scan 60 times per second so that the functional movements of heart muscle and lung tissue and the distribution of roentgen contrast medium in blood can be quantitated in any portion of the body, especially in the heart, great vessels, and lungs. The system is under evaluation as a research tool for physiologic and, ultimately, clinical investigations.

provides repetitive synchronous measurements of structural and functional parameters throughout individual cardiac or respiratory cycles. The DSR differs from commercially available CT scanners in that it images a volume rather than a slice, images the volume in stop-action, which minimizes blurring due to motion, and repeats the scan 60 times a second.

The DSR system is made up of four major subsystems: (i) the x-ray scanner (usually called the DSR), (ii) the video image storage system, (iii) the reconstructor computer, and (iv) the display and analysis system. Operationally, there are three phases to the use of the DSR system: (i) scanning, (ii) reconstruction, and (iii) display and analysis. Each of the four subsystems will be discussed in the following sections and related to the three phases of operation.

The assembly for the multiple x-ray scanner, the largest component of the DSR system, was installed in our laboratory in August 1979, and the first scans, which were made with a living dog, were performed in January 1980. The following discussion describes the system as of May 1980, and its preliminary applications.

Dynamic Spatial Reconstructor Scanner

The distinctive feature of the DSR is that it is a multiple x-ray tube, cone beam CT scanning system. Each x-ray cone beam transilluminates a volume (such as the thorax and its contents) and produces a two-dimensional projection image on a hemicylindrical fluorescent screen. The fluorescent image projected from each x-ray focal spot is acquired by a rapidly gated, intensified video camera located diametrically opposite the x-ray source, and is stored for subsequent processing. Rapid sequential actuation of the multiple x-ray sources and cameras, which may be considered as virtual two-dimensional detector arrays, allows short aperture times and acquisition at high repetition rates of the x-ray projection data, from which images of multiple transverse cross sections may be reconstructed.

The DSR depends on several modern technologies, including low-light-level, high-contrast video cameras; low-lag, rare-earth fluorescent screens; low-noise, wide-bandpass amplifiers; wide-band, low-noise video disk recorders; high-speed digital computation equipment; and sophisticated mathematical reconstruction algorithms. Indeed, the implementation of the DSR is the result of a closely coordinated multidisciplinary effort (*1*, *2*).

The scanner consists of a rotating structure (gantry) on which are mounted the x-ray tubes, hemicylindrical fluorescent screen, video cameras, and related electronics (Fig. 1). It is supported by a single X bearing, shown at the right of the patient's feet in Fig. 1, and is attached to the vertical face of the stationary support mounted on the floor.

The rotating structure turns on a horizontal axis of the recumbent experimental animal or patient at 15 revolutions per minute, that is, 1 revolution every 4 seconds. Rotation permits generation of more angles of view than can be obtained with the stationary configuration. Maximum obtainable resolution of the reconstruction image varies approximately as 1.5 times the number of views used (*3*).

An animal or patient subject to be scanned is separated from the rotating structure by a stationary tunnel, which is cantilevered from a supporting wall and which in turn supports a subject support system. This consists of a radiolucent table top that is bridged between two electrically controlled pedestals and spans the target region in the patient-interface tunnel. The section of the tunnel through which the x-rays must pass is fabricated of 2-millimeter-thick carbon filament material that is both radiolucent and mechanically strong.

The entire cantilevered gantry weighs approximately 13 tons. All high-voltage and low-voltage a-c power, control signals, and video signals are transmitted between the rotating structure and the off-gantry components by means of slip rings. The high-voltage slip rings are oil-immersed and bipolar in order to minimize high-voltage breakdown problems (the maximum tube potential is 120 kilovolts). Very low electronic noise and

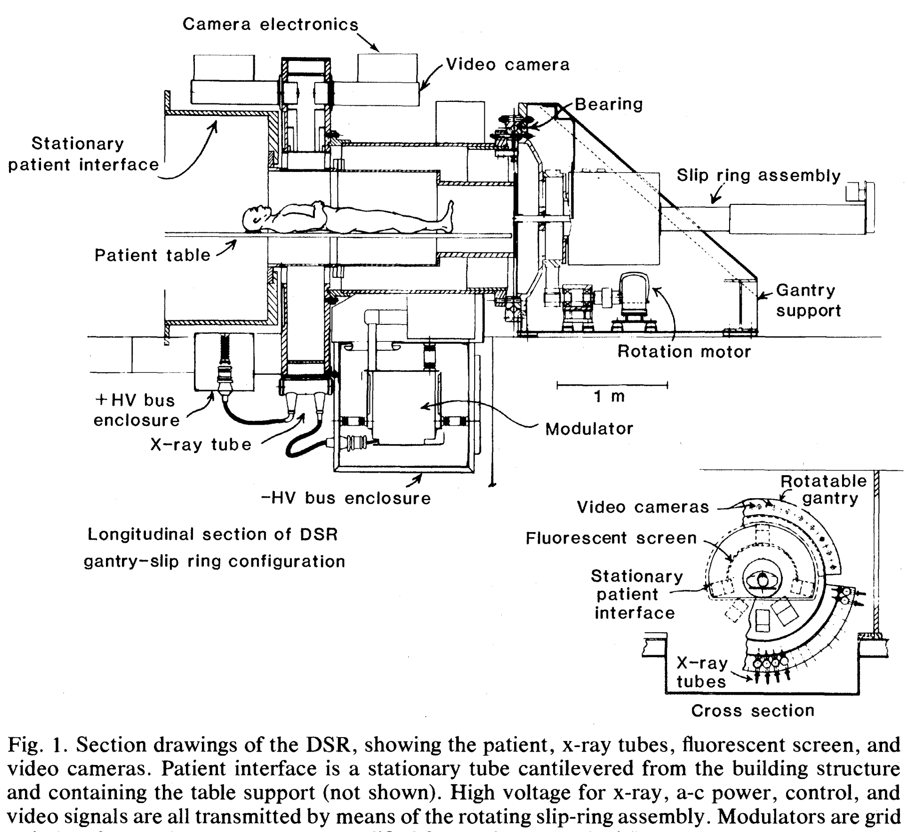

Fig. 1. Section drawings of the DSR, showing the patient, x-ray tubes, fluorescent screen, and video cameras. Patient interface is a stationary tube cantilevered from the building structure and containing the table support (not shown). High voltage for x-ray, a-c power, control, and video signals are all transmitted by means of the rotating slip-ring assembly. Modulators are grid switches for pulsing x-ray tubes. [Modified from Kinsey *et al.* (*24*)]

cross talk between video channels are provided at reasonable bandwidth with low-resistance triaxial-signal slip rings (signal-to-noise ratio = 80 decibels at 5 megahertz).

The 28 rotating-anode heavy-duty x-ray tubes (14 of which are installed at the time of writing) are positioned around 162° of arc on the rotating structure. Each of these tubes is capable of being pulsed at a peak input power of 100 kilowatts for approximately 350 microseconds every 1/60 of a second for a maximum duration of 20 seconds, at which time a cooling-off period is required. To minimize video storage requirements, the images from groups of four cameras are multiplexed 4 to 1 into a composite image containing only 60 of the 240 video lines from each of the four cameras.

The resulting seven multiplexed video images are recorded on the video disk recording system, which has a total of eight record/playback channels. Signal-to-noise ratio in the playback signal is about 50 dB at a 5-MHz bandwidth, which is adequate for reconstruction of the images of interest.

Control of the DSR is by means of an 8-bit microprocessor system, which can be operated directly through its own terminal or by high-level control (for instance, by on-line analysis of hemodynamic parameters of the subject being scanned) from a larger computer.

Computational Considerations

X-ray CT images are computed from measurements of the attenuation of x-rays transmitted through the body from many different angles of view. The mathematical algorithm applied to these measurements results in an approximate reconstruction of the spatial distribution of x-ray-attenuation densities within the section (or slice) scanned. The mathematical principles on which the transaxial reconstruction technique is based have been described in detail (*4, 5*).

Procedures for DSR scans differ from those for conventional CT scans in several ways, and special considerations are necessary in the application of the available reconstruction methods.

First, a cone beam (rather than a fan beam) of x-rays is used to allow synchronous imaging of a volume. The DSR geometry permits the divergent cone beam to be reasonably approximated by assuming that it consists of multiple parallel fan beams stacked in the axial direction. The 240 adjacent horizontal video lines, which constitute the projection image produced by the DSR at any angle of view, represent x-ray projections of near-parallel sets of fan beams. Useful reconstructions over the entire anatomic extent of organs such as the heart are then achieved by using conventional fan beam reconstruction formulas applied separately to the data obtained from each video line in the projection image (*6*).

A second important difference between DSR and conventional CT scans is that, in its highest temporal resolution mode of scanning (60 volumes imaged per second), the DSR will produce only 28 views over a limited 162° range. Furthermore, it images a cylindrical volume only 21.4 centimeters in diameter and 21.4 cm high, so that objects larger than this size (most adult chests) will exceed the field of view. Despite the limited number of views, limited field of view, and limited range of views in the highest temporal resolution mode of operation, useful reconstructions can be obtained from such data sets (*6*).

The problem of the limited field of view can be partially alleviated by performing target or "zoom" reconstructions; that is, only the region of the body containing the object of interest (such as the heart) is reconstructed. We have also implemented a technique developed by Lewitt (*7*) to correct mathematically the projection data recorded from a limited field of view before they are reconstructed.

When lower temporal resolution is acceptable, these problems of limited data sets can be minimized. Appropriate combination of the projection data obtained during rotation of the DSR provides more views for improved spatial resolution (for instance 112 views in 1/15 second) or wider views for reconstruction of subjects with transverse diameters up to 38 cm (*2*). This illustrates another powerful feature of the DSR, in that this rear-

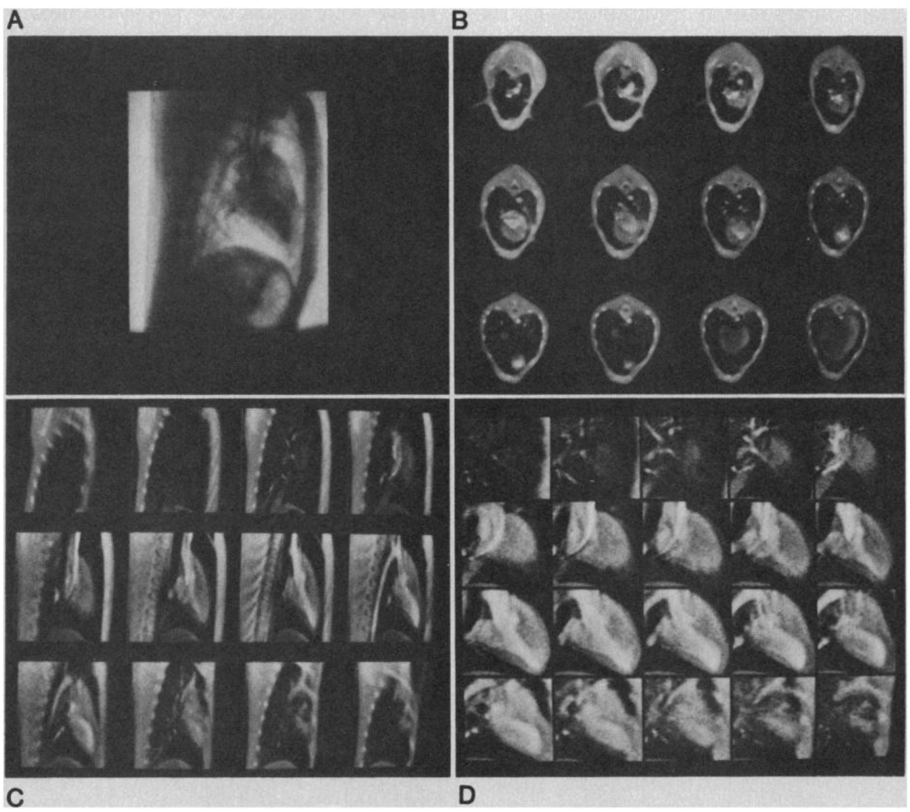

Fig. 2. (A) X-ray projection image of dog thorax during injection of contrast material into heart recorded at one angle of view during rotation of DSR. (B) Twelve 2-mm-thick cross sections of full thorax, 6 mm apart, extending over base to apex of heart. Curved line is the convex aluminum "table" on which the animal was supported during the scan. Bifurcation of the airway posterior to the heart, the descending aorta, and the left ventricular chamber in the heart can be readily identified. In the lower row of cross sections, the contrast medium (*8*) highlighted the apical portion of the left ventricular chamber, and the inferior vena cava and many pulmonary vessels are identifiable. (C) Twelve 2-mm-thick sagittal sections, 15 mm apart, computed from 128 1-mm-thick transverse sections. Upper row shows some of the blood vessels in the right lung. Middle row shows several sections through the heart in which the left ventricular chamber can be seen, along with the superior vena cava (first two images) and the aorta (fourth image). Bottom row shows vascular detail in the left lung. (D) Twenty 2-mm-thick sagittal zoom reconstructions of the heart region, 1 mm apart. The borders of the left ventricular chamber and ascending aorta are clearly discernible in this higher resolution reconstruction.

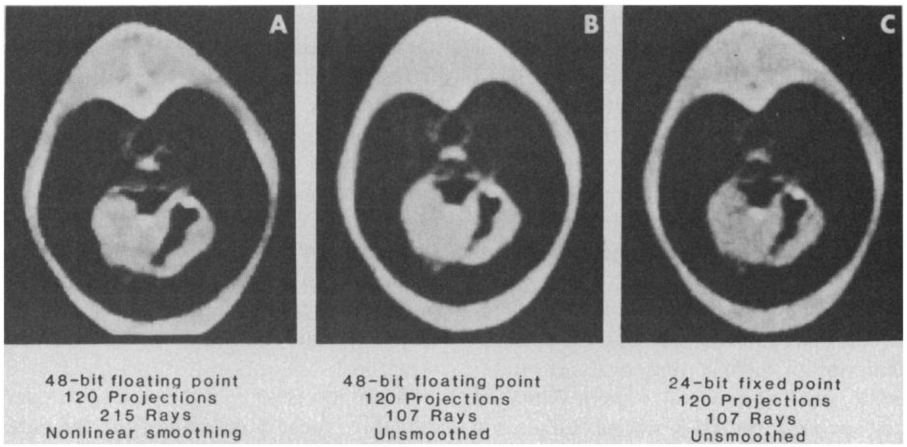

Fig. 3. Effects of various implementations of reconstruction algorithm on gray scale and spatial resolution of final image. (A and B) Images reconstructed by serial processing implementation on a commercial computer. (C) Image reconstructed by simulating a parallel processing computer. Images B and C are nearly identical; this verifies that the parallel processing computer will produce images without additional degradation, but with much less computation time. [Reproduced with permission from Swartzlander *et al.* (*25*)]

rangement of the data can be accomplished retrospectively (after the scan) in accord with the spatial, contrast, and temporal resolution requirements for the structures or functions of primary interest.

Figure 2 shows preliminary results obtained from the DSR by use of some of these techniques. The scan was performed on a live, intact dog approximately 4 seconds after x-ray contrast medium (*8*) was injected into the inferior vena cava. With only seven x-ray source and video camera systems, the full cone beam x-ray images from 112 successive angles of view over 166.5° were recorded in a total of 0.26 second and used to reconstruct multioriented sections over the entire anatomic extent of the thorax.

Although the cross-sectional images in Fig. 2 are 2 mm thick and 6 mm apart, other cross sections can be retrospectively varied in thickness and separation. This is achieved by averaging together any selected number of adjacent 1-mm-thick cross sections reconstructed from successive horizontal video lines over the entire anatomic extent of the thorax.

High-Speed Reconstruction

The data acquisition and processing requirements of this project are such that special-purpose, high-speed data processing devices are needed to permit users of the DSR to evaluate the image data within a reasonably short period after the scan is completed. For instance, the DSR gantry mechanism, operating at full capacity, is capable of collecting x-ray projection data sufficient to reconstruct images of up to 240 adjacent 1-mm-thick cross sections of the body every 1/60 second for up to 20 seconds. These data acquisition rates are nearly 10,000 times greater than those of commercial CT scanners, equivalent in digital terminology to 5.2 million 8-bit samples each 1/60 second, or 310 million samples per second. By comparison, the Landsat III earth resources satellite transmits images to its receiving stations at a rate roughly equivalent to 2.5 million samples per second—less than 1 percent of the rate of DSR data transmission.

Processing such large quantities of information creates a tremendous computational problem. In addition, the currently employed computer-based image reconstruction algorithms must perform several hundred arithmetic steps (primarily multiplications and additions) to calculate the brightness value of each of the 16,000 to 64,000 reconstructed image points or pixels that represent the array of volume elements (voxels) contained in a single cross-sectional image. Conventional computers reconstructing each cross section within several minutes would require up to 50 days to compute the images that can be reconstructed from a 1-second DSR scan. However, the time between the collection of the raw data and the presentation of the final results should be only a few minutes to maintain useful "feedback" between the observer and the patient or experimental animal under study.

To achieve this goal, we have designed and are fabricating special-purpose computers, exploiting advanced digital device technology, in which the arithmetic processes are tailored to extract maximum performance from the algorithms. A few minutes of processing for data collected within a few seconds will require at least 3×10^9 arithmetic operations per second, even assuming a computationally efficient reconstruction algorithm (*9*). A considerable increase in processor throughput can be attained by replacing conventional serial-computation image reconstruction algorithms by as much parallel arithmetic as possible. A parallel processing version of the reconstruction algorithm was developed in which groups of the 28 x-ray image projections produced simultaneously are each subjected to a "linear filtration" process; they are then "back-projected" (added together) simultaneously to generate each pixel of the image being reconstructed (*9*).

To verify the validity of this approach, the parallel processing algorithm was simulated on a general-purpose computer to a very high level of detail, including several specific implementations of its arithmetic developed to improve the overall computational efficiency (*9*) and the precision employed in all arithmetic calculations. These simulations (Fig. 3) demonstrated that the parallel processor would generate images equal in quality to those obtained with the conventional serial-computation approaches, assuming identical sets of input data. For even greater throughput, the parallel processor is being fabricated with high-speed subnanosecond emitter-coupled logic, a family of digital logic whose individua devices achieve speeds four to five times greater than that of conventional components (*10*).

The parallel nature of the reconstruction processor and the flexibility of its control unit (*11*) allow use of several alternative versions of the algorithm. These will, for example, permit (i) direct computation, from multiple transverse-section data, of additional sections oriented at any desired angle relative to the orthogonal body axis, or (ii) higher spatial resolution (zoom) images of any desired smaller volume within the original volumetric reconstruction.

Display and Analysis of Image Data

Display and quantitative analysis of the time-varying three-dimensional image and associated parametric data generated during a single, several-second scanning period of the DSR presents difficult problems technologically and with respect to human sensory input and comprehension. These problems arise primarily because of (i) the significant number of cross-sectional images generated during a scanning procedure and (ii) the fact that the transverse cross-sectional images, which are the output of the scanning and reconstruction process, are often not well suited to quantitative analysis of the shape and dimensions of the structures being studied.

For example, measurements that can be made in a plane, such as cardiac wall thickness or aortic valve area, must be made in the appropriate plane, which may be oblique to the original transverse sections scanned. The correct location and orientation of such an oblique plane relative to the organ under study can best be determined by viewing it within the volume image. Ideally, the investigator should be able to select the correct plane by using operator-interactive multidimensional display capabilities. How well this problem can be handled will be a major determinant of the practicality of the DSR for diagnostic or investigative use.

Some preliminary attempts to solve this problem involve new display techniques that allow the observer to view directly the unedited (*12*) volume image. Of particular interest is a display method termed projection (*13*), which enables the observer to view the volume reconstruction image data from any desired angle. This method involves mathematical projection (summation along a set of ray paths) of the volume image onto a plane. The resulting two-dimensional projection images can be displayed on a television monitor, as shown in Fig. 4B. Before projection, the reconstructed volume can also be mathematically rotated to permit viewing of the reconstruction from any desired angle (Fig. 4D). Projection images formed at angles of view corresponding to binocular disparity (approximately 6° apart) can be viewed as a stereo pair to permit visualization of the volume image in three dimensions, as illustrated in Fig. 5.

Display of the stack of parallel cross-sectional images as a volume image presents a dilemma: the volume image may defeat (undo) the primary advantage of the single cross-sectional CT image, which is that it overcomes the obscuring effect of superposition of bodily organs. However, by selective reduction of the brightness value of selected image voxels before projection and display, it is possible to effectively overcome the obscuring effect of superposition and still allow the three-dimensional anatomy of the structure of interest to be visualized, as illustrated in Fig. 4C. These methods, referred to as numerical dissection or selective tissue dissolution, involve total removal or dimming of selected picture elements to enhance the visibility of remaining image data.

Preliminary applications of these techniques indicate that they greatly facilitate determining the orientation and location of "invisible" anatomic structures in a three-dimensional reconstruction, although they are rather incon-

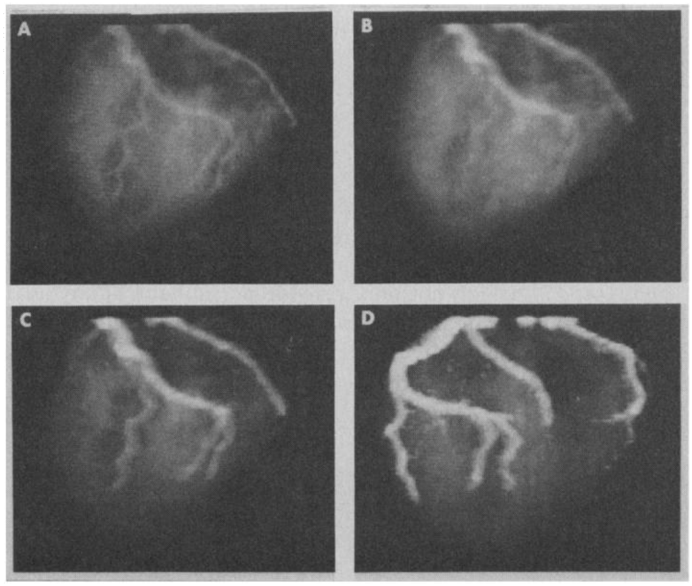

Fig. 4. Projection images for conveying three-dimensional anatomy of coronary arterial tree. Base of heart is at the top, apex at the bottom in each panel. (A) Digital display of radiograph of isolated canine heart with x-ray contrast medium in coronary arteries. (B) Computer - generated projection of volume reconstruction of the same canine heart. This two-dimensional image, generated from the three-dimensional image data obtained by the transaxial reconstruction process, is slightly blurred but otherwise identical to the radiograph. (C) Before projection, the intensity of the heart wall was selectively reduced, leaving the coronary arteries relatively brighter and more visible. This technique cannot be applied to the radiograph. (D) Same partially dissolved image data as in (C), but projected from a different angle of view. This image clearly shows the septal (central) coronary artery, which was obscured by the circumflex (left) coronary artery in (C). In (C) and (D) the dissolution was 83.5 percent; the angle of rotation was 0° and 45°, respectively.

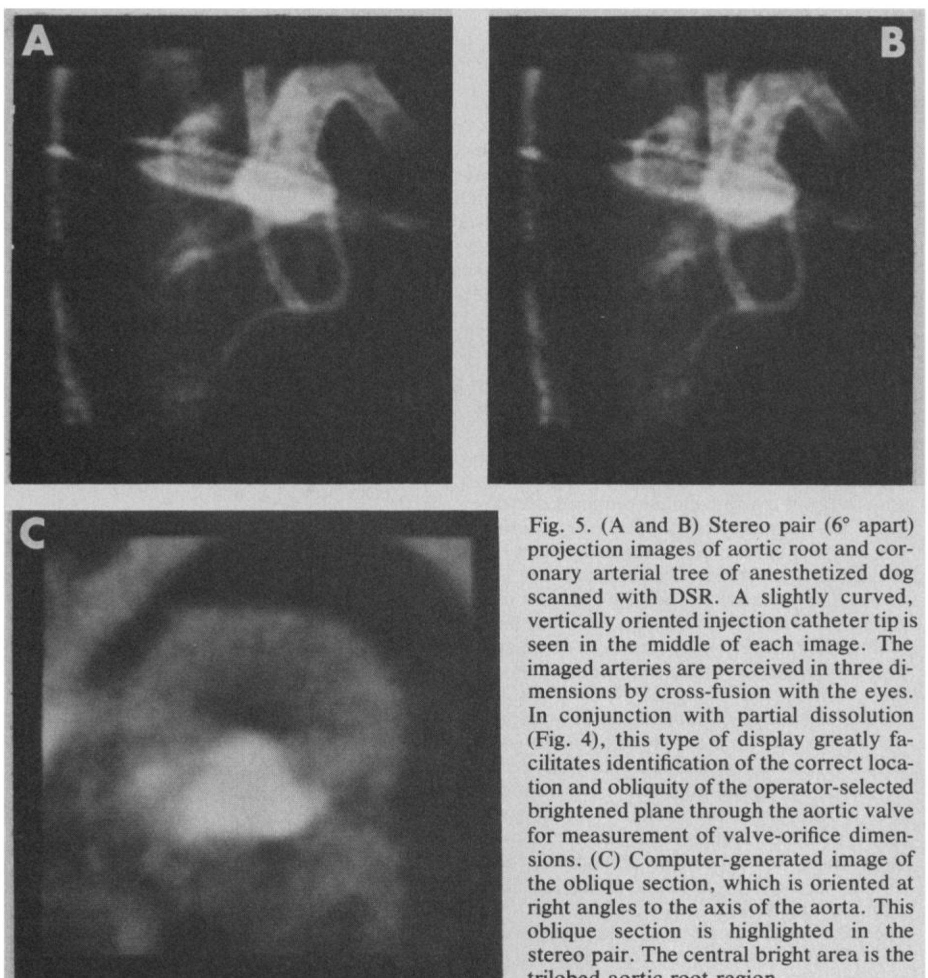

Fig. 5. (A and B) Stereo pair (6° apart) projection images of aortic root and coronary arterial tree of anesthetized dog scanned with DSR. A slightly curved, vertically oriented injection catheter tip is seen in the middle of each image. The imaged arteries are perceived in three dimensions by cross-fusion with the eyes. In conjunction with partial dissolution (Fig. 4), this type of display greatly facilitates identification of the correct location and obliquity of the operator-selected brightened plane through the aortic valve for measurement of valve-orifice dimensions. (C) Computer-generated image of the oblique section, which is oriented at right angles to the axis of the aorta. This oblique section is highlighted in the stereo pair. The central bright area is the trilobed aortic root region.

venient because of the very slow operator interaction possible at present. For operator interaction to be useful, a system used to display these data in three or even four dimensions must allow the observer to interact—that is, "cut," "peel," or remove obscuring structure—and subsequently measure distance, area, or "density" in a manner and time scale similar to those in which the surgeon or pathologist interacts with the real body. There is reason to believe that this can be achieved with display systems such as those based on a variable focal length (varifocal) optical element (*14, 15*), which not only provide a true three-dimensional image but can be made operator-interactive.

Three-Dimensional Indicator-Dilution Curves

Over the last four decades, indicator-dilution curves, recorded as concentration versus time from various sites in the cardiovascular system, have provided one of the most powerful tools for study of cardiac, circulatory, and capillary exchange dynamics in organs and structures of the body.

The capability of the DSR to obtain, in 1 second, 60 noninvasive measurements of both the total amount and the concentration of contrast medium in a known volume at any anatomic site in the body adds new dimensions to circulatory indicator-dilution techniques. By computer manipulation of the image data, the position, shape, and dimensions of the sampling volumes can be varied retrospectively from a few cubic millimeters up to the full synchronous scanning volume of the DSR, within the geometric limits of this scanned volume. Furthermore, sampling regions can be made to vary with time to conform continuously with the shape, dimensions, and position of moving structures such as the lungs, myocardium, and cardiac chambers.

Synchronous volumetric reconstructions will allow measurement of the total volume of the lumens between multiple sampling sites in branching vascular segments. The average flow in a segment can then be calculated by dividing the volume of its vascular lumens by the average mean transit time of a mixture of contrast medium and blood between the sampling site in the input vessel to the segment and the sampling site in its branches (*16*). Another, more powerful, method for estimating blood flow in a vessel relative to each of its downstream branches is based on measurement of the fraction of indicator transported by each vessel (*17*). For this application, the ratios of the blood flows in the branches are proportional to the ratios of the areas of the dilution curves recorded for each sampling site.

Even more exciting is the potential of the DSR for studies of the spatial distribution dynamics of blood flow and content in any region of the body. These possibilities relative to the lungs are illustrated in Fig. 6, for which a highly invasive stratagem was used to provide a pictorial representation of what can be done with the DSR noninvasively, as indicated in Fig. 2. Following an intravenous injection of contrast medium, the changes in x-ray density (dilution curves) for every reconstructed volume element throughout the anatomic extent of, for example, the thorax, can be computed and plotted against time during transit of this circulatory indicator through the reconstructed volume.

The same principle forms the basis for noninvasive measurements of the spatial distribution dynamics of pulmonary ventilation throughout individual respiratory cycles. For this application, no injection of contrast medium is required since essentially zero x-ray density of the respiratory gases serves as the x-ray indicator.

The sampling assumptions that are inherent (but violated) in estimates of cardiac output by conventional applications of the direct Fick and indicator-dilution methods also pertain to three-dimensional dilution curves derived from DSR

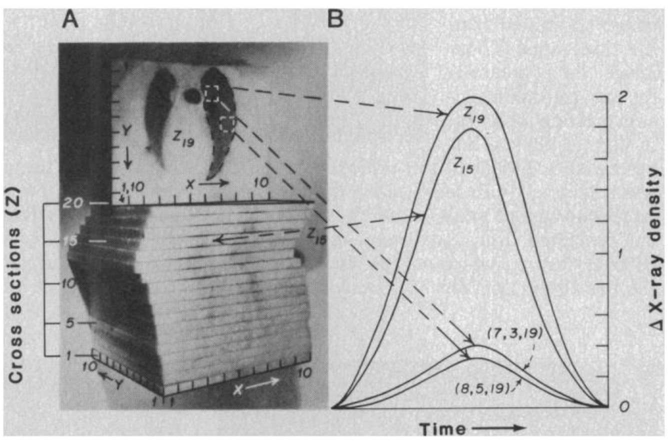

Fig. 6. Schematic showing capabilities of the DSR for noninvasive measurements of spatial distribution dynamics of pulmonary blood flow. (A) Photographic representation of the information stored in the computer from multiple reconstructed transverse section images after a single volumetric scan of the thorax. The chest wall and mediastinal structures have been removed by numerical tissue dissolution (*13*). Sixty volumetric scans can be made in 1 second, and each scan provides additional sets of image information during transit of x-ray contrast medium through the pulmonary circulation after injection into a peripheral vein. (B) The change in x-ray density of every three-dimensional picture element throughout the lungs can be plotted against time, as illustrated in the lower right traces for two of these voxels, identified by their X, Y, and Z spatial coordinates. Similarly, x-ray-density dilution curves can be plotted for the cross sections, which are identified by their respective Z coordinates, as illustrated in the top two traces in (B) for cross sections Z_{15} and Z_{19}.

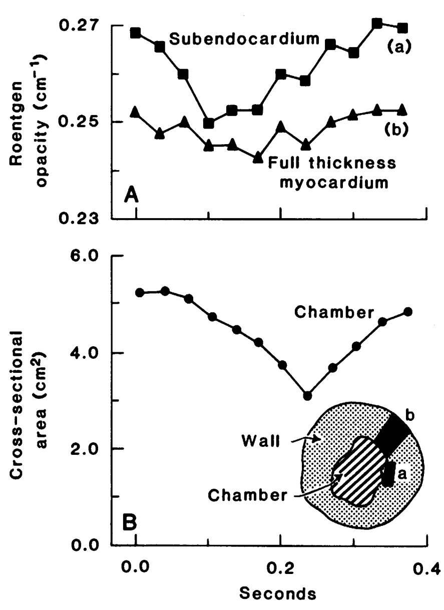

Fig. 7. Data derived from a 30-per-second sequence of computer-generated images of one transverse section of an anesthetized dog's left ventricle. The images were generated with a prototype scanner having a single x-ray source (*1*); the arrangement required use of a gated scanning procedure (*6*) during continuous infusion of roentgen contrast medium into the left atrium. (A) Signals from sampling windows. The increase of roentgen opacity over the value of approximately 0.2 cm^{-1} for heart wall before injection of contrast medium is proportional to the amount of blood in the region of heart wall sampled. Preferential decrease of opacity in subendocardial region is consistent with well-documented preferential compression of subendocardial wall during systole. (B) Initial constant cross-sectional area of left ventricular chamber during isovolumic phase of systolic contraction followed sequentially by decreasing area during ejection phase and increasing area during filling phase of one average heart cycle. (Inset) Size and location in heart wall of image brightness (sampling) windows. [Adapted from illustration in (*23*)]

scanning data (*18, 19*). However, it is important to remember that the accuracy of conventional applications of the direct Fick and indicator-dilution methods is generally considered the "gold standard" in clinical medicine today. It is hoped that by adding new dimensions (sampling volumes with selectable shape, dimensions, position, and time) to indicator-dilution methodologies, the DSR will prove to be comparable to or of even greater value than the current Fick and Stewart-Hamilton techniques.

Cardiac Structure and Function

One of the major objectives of the DSR design is to permit accurate measurement of the structure and function of the diseased and normal heart, at rest and during stress. Other investigators, using casts of heart chambers (*20*) and arrested dog-heart preparations (*21*), have demonstrated the potentially great accuracy of x-ray CT imaging for estimation of heart chamber volume and size of regions of dead heart muscle, respectively. These studies were carried out with "single-slice" slow CT scanners and postmortem preparations by procedures not suitable for clinical diagnosis. The DSR will permit accurate use of cardiac and circulatory x-ray CT imaging techniques in awake, unanesthetized humans.

For evaluation of the heart as a pump, the total mass of the heart muscle and the volume of the heart chambers can be calculated from multiple, parallel images such as those illustrated in Fig. 2. These data can be obtained each 1/60 second throughout one heartbeat. Preliminary results indicate that this technique provides accurate estimates of the volume of blood pumped by the heart. Regional function of the heart wall during the phase of forceful emptying of the heart chambers has been shown to be a good index of the blood supply to the heart wall (*22*). The repetitive, synchronous volumetric imaging capability of the DSR makes possible measurement and evaluation of heart wall thickening over all regions of the heart.

One important clinical problem in need of new insights is ischemic heart disease, the major cause of heart attacks. This disease often involves localized narrowing of one or more major coronary arteries, each of which supplies blood to large portions of heart muscle. The severity of impairment of the heart's pump function depends on how much of the total heart wall has been damaged as a result of reduced blood flow through the narrowing.

A DSR scan performed during the injection of contrast medium into the blood passing through the heart's chambers and coronary arteries makes possible simultaneous evaluations of the location and severity of narrowing in all of the coronary arteries; the location and severity of reduction of blood supply to, and amount of movement in, all regions of the heart wall; and the total amount of blood pumped by each beat of the heart during the scanning procedure.

Localized narrowing—less than 0.5 mm in diameter—in coronary arteries that are 1 to 3 mm in diameter represents a major threat to the viability of heart muscle and hence to heart function. Such small diameters cannot be measured with adequate accuracy because of the blurring effect of the imaging and reconstruction process. However, some of these blurring effects can be largely "undone" by image-processing techniques, so that fairly accurate estimates of the percentage of narrowing of a major coronary artery can be made (*23*). In addition to the detection and evaluation of coronary artery narrowing, the same injection of contrast medium can be used to show the location and extent of regions of heart wall to which the supply of blood has been interrupted or diminished by an occlusion or narrowing of the coronary arteries. Preliminary studies indicate that cyclic changes of regional myocardial blood content can be imaged with the DSR (Fig. 7).

DSR-based evaluation of other acquired and complex congenital abnormalities of the heart and great vessels should also be possible with greater accuracy and less invasion than are obtainable with current clinical techniques. Research planned for the next few years is aimed at evaluating whether such diseases can be detected earlier and measured more accurately than is currently possible. If they can, it is reasonable to expect that the natural progression of these diseases will be better understood and that appropriate therapy can be instituted at earlier stages of the disease process, thereby reducing risk of irreversible damage to the heart.

Conclusion

Over the next 2 to 3 years the capabilities of the DSR will be evaluated. We hope to determine how accurately the DSR can be used to estimate the spatial distribution of myocardial and pulmonary perfusion and pulmonary ventilation, and the three-dimensional anatomy and hemodynamics of complex congenital cardiac and great vessel defects. Once these capabilities have been defined, physiologic questions of a higher order and more difficult pathophysiologic problems can be addressed. For instance, in patients with aortic valve stenosis, is the accurate measurement of the magnitude or rate (or both) of increase in left ventricular hypertrophy sufficient information to determine that the defective valve should be replaced and when the operation should optimally be performed? We expect some of these studies to indicate that current conventional single-modality diagnostic techniques (such as coronary angiography), which measure limited aspects of structure or function, provide information that is inadequate for accurate diagnostic and therapeutic decisions concerning the complex problems presented by ischemic heart disease.

The goal of these research activities is primarily to provide insights into normal and pathophysiologic processes. Consequently, the DSR could be seen as a national resource whose object is to facilitate studies of dynamic interrelationships of biologic structures and their function in intact experimental animals and probably eventually in humans with disabilities related to the heart, lungs, or the circulation in any region of the body.

References and Notes

1. R. E. Sturm, E. L. Ritman, S. A. Johnson, M. A. Wondrow, D. I. Erdman, E. H. Wood, *Proc. San Diego Biomed. Symp.* **15**, 181 (1976).
2. E. L. Ritman, J. H. Kinsey, R. A. Robb, L. D. Harris, B. K. Gilbert, *Am. J. Roentgenol.* **134**, 369 (1980).
3. R. H. Huesman, *Phys. Med. Biol.* **22**, 511 (1977).
4. R. Gordon and G. T. Herman, *Int. Rev. Cytol.* **38**, 111 (1974).
5. L. A. Shepp and J. B. Kruskal, *Am. Math. Mon.* **85** (No. 6), 420 (1978).
6. R. A. Robb and E. L. Ritman, *Radiology* **133**, 655 (1979).
7. R. M. Lewitt, *Med. Phys.* **6** (No. 5), 412 (1979).
8. Contrast medium is an iodine-containing fluid that, when injected into the bloodstream, greatly reduces x-ray transmission through blood. It highlights circulatory structures in x-ray images, particularly during the transient rapid phase of its first transit through the cardiac chambers, arteries, and veins. Blurring due to motion and inability to scan the entire organ synchronously with current CT scanners prevent adequate imaging of this first transit with its high information content.
9. B. K. Gilbert, A. Chu, D. E. Atkins, E. E. Swartzlander, Jr., E. L. Ritman, *Comput. Biomed. Res.* **12**, 17 (1979).
10. B. K. Gilbert, L. M. Krueger, R. D. Beistad, *IEEE Trans. Components Hybrids Manuf. Technol.* **CHMT-3** (No. 1), 125 (1980).
11. B. K. Gilbert and L. D. Harris, *IEEE Trans. Nucl. Sci.* **NS-27** (No. 3), 1197 (1980).
12. Unprocessed or raw reconstructed three-dimensional array of x-ray density values.
13. L. D. Harris, R. A. Robb, T. S. Yuen, E. L. Ritman, *J. Comput. Assist. Tomogr.* **3**, 439 (1979).
14. H. Mark and F. Hall, *Proc. Soc. Photo-Opt. Instrum. Eng.* **120**, 192 (1977).
15. R. L. DeMontebello, *ibid.*, p. 184.
16. H. C. Smith, R. E. Sturm, E. H. Wood, *Am. J. Cardiol.* **32**, 144 (1973).
17. B. M. T. Lantz, D. P. Link, J. M. Foerster, J. W. Holocraft, *Acta Radiol. Diagn.* **21**, 3 (1980).
18. M. B. Visscher and J. A. Johnson, *J. Appl. Physiol.* **5**, 635 (1953).

19. E. H. Wood, D. Bowers, J. T. Shepherd, I. J. Fox, *ibid.* **7**, 621 (1955).
20. M. J. Lipton, T. T. Hayashi, D. Boyd, E. Carlsson, *Radiology* **127**, 415 (1978).
21. P. T. Siemers, C. B. Higgins, W. Schmidt, W. Ashburn, P. Hagan, *Invest. Radiol.* **13**, 103 (1978).
22. J. H. Chesebro, E. L. Ritman, R. L. Frye, H. C. Smith, B. D. Rutherford, R. E. Fulton, J. R. Pluth, D. A. Barnhorst, *Circulation* **57**, 952 (1978).
23. J. G. Scanlan, D. E. Gustafson, P. A. Chevalier, R. A. Robb, E. L. Ritman, *Am. J. Cardiol.*, in press.
24. J. H. Kinsey, R. A. Robb, E. L. Ritman, E. H. Wood, *Herz* **5** (No. 3), 177 (1980).
25. E. E. Swartzlander, Jr., and B. K. Gilbert, *Proc. Soc. Photo-Opt. Instrum. Eng.* **119**, 299 (1977).
26. We thank our colleagues in the Departments of Physiology and Biophysics, Cardiology, and Radiology and members of our National Advisory Committee for their support, and especially our technical and computer programming staff, who made this project reality. The work of our secretarial and artistic staff in the preparation of this manuscript and of voluminous grant requests has been indispensable. This project was supported by the National Institutes of Health through NHLBI program project grant HL-04664 and DRR grant RR-00007, the Fannie E. Rippel Foundation, and several other contributors.

Endoscopy: Developments in Optical Instrumentation

Max Epstein

The endoscope, whose name was derived from two Greek words—endon, within, and skopein, to view—has become an important and versatile tool in medicine. It allows for remote viewing, photography, biopsy, and even surgery on organs and tissue, since it can be passed through natural openings and cavities in the human body or through the skin, that is, percutaneously. Consequently, new medical procedures such as bronchoscopy, gastroscopy, proctosigmoidoscopy, and so forth, have evolved. While most of these procedures are part of particular medical specialties, the principles of operation and basic features of the various instruments used are similar.

Summary. Optical fibers transmit high-intensity illumination for viewing internal organs and tissue. Remote viewing is obtained by relays of lenses or graded-index-of-refraction rods in rigid endoscopes and by precisely aligned fiber-optic bundles in flexible fiberscopes. Endoscopy is considered for routine examinations, such as in colonoscopy. Lasers are used as surgical tools through endoscopes for cutting and coagulation. They may also be used to provide illumination for the efficient transmission of light through thin optical fibers.

The background, physical principles, and applications of the endoscope have been described (*1*). Briefly, an endoscope embodies the means for transmitting light to illuminate the internal space being viewed and for conveying the image of the distal object back to the viewer. In addition, most endoscopes have ancillary channels for passage of air, water, and implements such as biopsy forceps, cytology brushes, or various surgical tools that can be remotely controlled. The manner in which the image is conveyed determines whether the instrument is rigid or flexible; for example, the transmission of images by a relay of lenses requires that the endoscope remain rigid, while the use of a bundle of precisely aligned optical fibers makes a flexible endoscope, often referred to as a fiberscope. For the transmission of light for illumination of the distal objects, nearly all current endoscopes use optical fibers.

The author is professor in the Department of Electrical Engineering and Computer Science, Northwestern University, Evanston, Illinois 60201.

Optical Fibers for Illumination

Figure 1A shows the trajectories of rays entering a glass rod of refractive index n_1. Ray I_1, upon refraction at the entry face, is totally reflected at the wall of the glass rod and propagates along the rod by repeatedly bouncing off the wall until it refracts and emerges at the exit face. On the other hand, most of ray I_2 does not reflect at the wall of the rod but, instead, refracts and escapes through it. All rays entering at an angle smaller than α_0 such that they impinge on the wall at an angle greater than the critical angle α_c, will be trapped in the rod and continue to its exit face. This feature of light guiding holds even if the glass rod is bent at a radius substantially larger than the diameter of the glass rod, and the angle α_0 determines the aperture or the cone of light accepted and transmitted through such an optical fiber. Since any contact with the outside wall of the rod or fiber will affect and impair the total reflection and, thus, the trapping of light rays, it is customary to enclose the glass rod or fiber in a tube of glass of lower refractive index $n_2 < n_1$ (Fig. 1B). The interface between the two glasses causes the reflections to be nearly lossless; however, the critical angle is greater, and the numerical aperture (NA) of the clad or step-index optical fiber is smaller than in the case of an unclad rod and is given by

$$NA = n_0 \sin\alpha_0 = (n_1^2 - n_2^2)^{1/2}$$

where n_0 is the refractive index of the surrounding medium and is equal to 1.0 for air and 1.33 for water.

When drawn in a furnace to a diameter of 25 or 50 micrometers, the clad optical fiber is quite flexible and can be bent to radii of less than 1 centimeter. In order to transmit adequate light, the thin optical fibers are gathered in a bundle with the ends bound and polished. Since relatively short lengths of a few meters are involved, the resultant attenuation of light is far below that available in the current low-loss fibers that are used in communication systems. Low-loss fibers have been developed that can efficiently transmit wide-band communication signals over large distances without amplification and with immunity to electromagnetic interference. An important feature that distinguishes the applications in illumination from those in communications is the need for a high-aperture fiber. Glass fibers with a core made of flint glass ($n_1 = 1.62$) and soda lime for the cladding ($n_2 = 1.52$) have an aperture of 0.56 which, in air, renders a cone of light of 68°. Since most imaging systems employ distal lenses and thus provide wide-